The Open University

Open Research Online

The Open University's repository of research publications
and other research outputs

Comparison of Back-Thinned Detector Ultraviolet Quantum Efficiency for Two Commercially Available Passivation Treatments

Journal Item

How to cite:

Heymes, Julian; Soman, Matthew; Randall, George; Gottwald, Alexander; Harris, Andrew; Kelt, Andrew; Moody, Ian; Meng, Xiao and Holland, Andrew D. (2020). Comparison of Back-Thinned Detector Ultraviolet Quantum Efficiency for Two Commercially Available Passivation Treatments. IEEE Transactions on Nuclear Science, 67(8) pp. 1962–1967.

For guidance on citations see FAQs.

© 2020 IEEE

Version: Accepted Manuscript

Link(s) to article on publisher's website:
http://dx.doi.org/doi:10.1109/TNS.2020.3001622

Copyright and Moral Rights for the articles on this site are retained by the individual authors and/or other copyright owners. For more information on Open Research Online's data policy on reuse of materials please consult the policies page.

oro.open.ac.uk

Comparison of Back-thinned Detector Ultraviolet Quantum Efficiency for Two Commercially Available Passivation Treatments

Julian Heymes, Matthew Soman, George Randall, Alexander Gottwald, Andrew Harris, Andrew Kelt, Ian Moody, Xiao Meng, and Andrew Holland

Abstract—**Back-thinned silicon detectors offer a high response over a very broad spectrum for direct detection by providing an efficient optical path into the sensing silicon avoiding front face structures manufactured from metal, polysilicon, nitrides and oxides that may absorb the incident light before reaching the sensing silicon.**

We have tested two CCDs with different back-surface shallow p+ implant thicknesses (basic and enhanced) at the M4 line (wavelength between 40 and 400 nm) at PTB's Metrology Light Source in Berlin. This characterisation in the ultraviolet spectral range extends the soft X-ray Quantum Efficiency dataset previously acquired with the exact same devices.

Due to the short absorption depth and the scope for many types of interactions of the device materials with ultraviolet photons, Quantum Efficiency measurement and stability of the device against extended exposure in the UV is of ongoing interest. Therefore, Quantum Efficiency measurements have been carried out before and after exposures to quantify any change in behaviour. To allow characterisation of the passivation processes only, the devices have no anti-reflection coating.

The measured Quantum Efficiency of the standard back-thinned CCD is below 10 % between 70 nm and 370 nm. An average additional 5 % efficiency is achieved in the enhanced device within the same range. At the limits of the measured spectrum, towards soft X-ray or towards the visible range, the Quantum Efficiency increases and the difference between the standard and the enhanced process is reduced as the photon absorption length increases beyond the immediate back surface. The measured Quantum Efficiency after long high fluxes exposures at 200 nm shows remarkable improvement.

Index Terms—**CCD, CIS, QE, X-ray, EUV, VUV**

I. Introduction

Achieving high Quantum Efficiency (QE) with back-thinned back-illuminated CCDs or CMOS image sensors requires post-processing steps adapted to the targeted spectral range of the application (from near infrared to soft X-ray). Thinning a device into low doped silicon to reduce the field free region between charge collection potential well and the back surface leads to a backside potential well that pulls shallow generated photoelectrons to the back surface where they are lost through surface recombination [1]. This potential well is sufficiently large to lose any signal generated by photons of short attenuation length (e.g. ultraviolet) resulting in zero Quantum Efficiency. In order not to lose the photogenerated charge, minimising the width of the potential well is required and can be achieved by passivation of the back-surface (see figure 2).

Another strong effect preventing high Quantum Efficiency is the reflectivity of the back-surface which still exists after passivation. This effect can be mitigated in some wavelength ranges with adequate anti-reflective coatings that will not be discussed in this paper.

In this paper, we will first describe the effects of the thick backside potential wells and of the reflectivity on the Quantum Efficiency in the ultraviolet spectral range from devices with no anti-reflection coating. The passivation method to minimize the dead layer will then be detailed. Two levels of this treatment, commercially offered by Teledyne-e2v, will then be compared through Quantum Efficiency characterisation using monochromatized synchrotron radiation between 40 nm and 400 nm, refined in the Vacuum UV (VUV) range. Measurements in such a broad range of wavelengths support testing of models for understanding and for the prediction of Quantum Efficiency. The measurements results as well as the effect of long exposures to a high flux of ultraviolet radiations on the treated back-surface will be discussed.

II. Direct Detection of Ultraviolet Radiation in Silicon

The ultraviolet spectrum corresponds to wavelengths between 10 nm and 400 nm. This range can be divided in three main subranges: near ultraviolet (NUV): 300 nm – 400 nm, middle ultraviolet (MUV): 200 nm – 300 nm, and vacuum ultraviolet (VUV): 200 nm – 10 nm. Within this spectrum, photons absorbed in the sensitive volume are converted to a variable number of electron-hole pairs (depending on the wavelength of the incident radiation) by the photoelectric effect.

A. Absorption Length

The absorption length expresses the distance after which the number of photons in a beam has been reduced to 1/e (37 %) of its original value. It is calculated across the spectral range using the imaginary part of the complex refractive index,

J. Heymes, M. Soman, G. Randall, X. Meng and A. Holland are with Centre for Electronic Imaging, The Open University, Milton Keynes, MK7 6AA, UK.

A. Gottwald is with Physikalisch-Technische Bundesanstalt, Abbestraße 2-12, 10587 Berlin, Germany.

A. Harris, A. Kelt and I. Moody are with Teledyne-e2v, 106 Waterhouse Lane, Chelmsford, CM1 2QU, UK.

E-mail: julian.heymes@open.ac.uk

The UV measurements presented in this paper were carried out at the Metrology Light Source, operated by PTB.

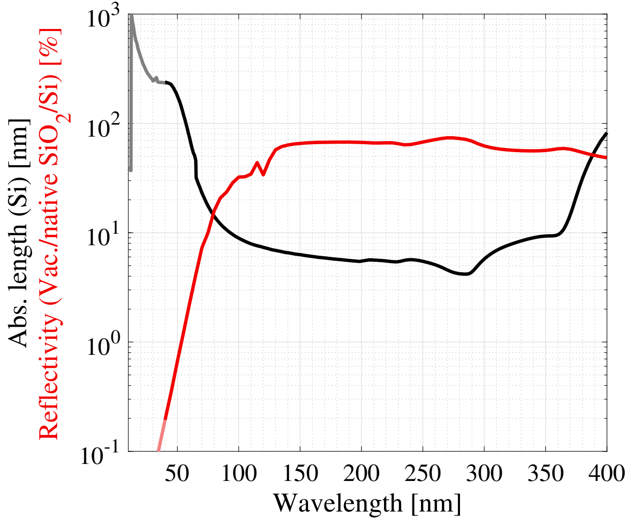

Fig. 1: Absorption length of Silicon (black) and reflectivity (red) of an uncoated device (Vacuum/Native Oxide/Silicon interface) in the ultraviolet spectral range. The attenuated colour below 40 nm represents the part of the ultraviolet spectrum for which no measurement has been performed in section III.

the extinction coefficient k, for the material studied (silicon data from [2], [3], [4]). Its values in the ultraviolet domain is shown as the black line in figure 1. The distance mostly does not exceed a few tens of nanometres within the range and is noticeably short (below 10 nm) for wavelengths between 90 nm and 360 nm. The minimum attenuation length is 4.2 nm for a 285 nm photon. For comparison, the absorption length at 400 nm is 82 nm.

Teledyne-e2v performed quantum efficiency measurements in the visible spectral range (above 400 nm) on an etched device without further processing [5]. No signal was measured for wavelengths below 450 nm. 90 % of the light at this wavelength is absorbed within 568 nm (using data from [3], [4] and $\approx$ 900 nm using the data in [6]). Therefore, the width of the potential well of an etched device without further processing is at least 568 nm resulting in zero Quantum Efficiency in the majority of the ultraviolet spectral range.

B. *Reflectivity*

In addition to the effects of short attenuation length, the surface of Silicon is reflective for radiation in the ultraviolet to near infra-red spectral range which significantly reduces the measured Quantum Efficiency. The vacuum/native oxide/Silicon reflectivity shown as the red curve in figure 1 has been obtained using the Macleod software with the refractive indices and absorption coefficients from [3], [4].

On uncoated devices, a reflectivity of more than 50 % is expected over a large range of the ultraviolet spectrum (127 nm–394 nm). Around 272 nm, about 74 % of the incident light will be reflected at the surface of the device.

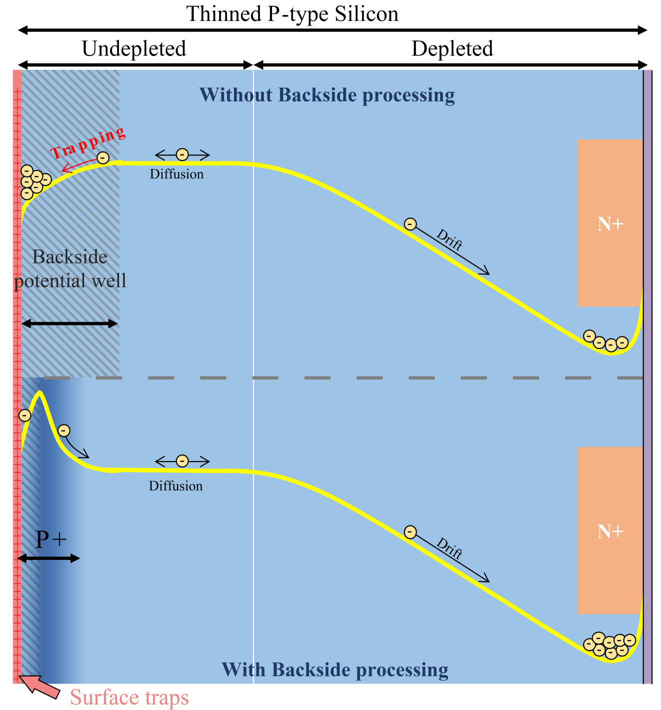

Fig. 2: Schematic representation of two back-illuminated thinned sensors. The top version presents no backside processing resulting in a thick backside potential well trapping a large proportion of the photogenerated charge. The bottom version presents backside P+ implantation reducing the potential well. The vertical scale represents the potential for the yellow line. The reader is referred to the online version for the coloured version.

C. *Quantum Efficiency Enhancement*

Increasing the Quantum Efficiency of back-illuminated thinned silicon-based sensors requires that the width of the backside potential well to be as thin as possible. This potential well is caused by the presence of surface traps due to the dangling bonds of the silicon crystalline structure left after etching and native oxide charge. The electrons photogenerated within this region are attracted towards the backsurface (see top part of figure 2) and recombined and are therefore lost.

A method to reduce the width of the potential well consists of adding a thin layer of higher doping concentration at the back-surface of the device. Molecular beam epitaxy has proven to be capable of forming ultra thin p+ layers of around 1 nm [7] but is not widely available for industrial processing.

The industrial passivation method commercially available at the wafer level from Teledyne-e2v is low-energy boron implantation. As the typical high-temperature annealing is incompatible with the image sensors structures composed of successive layers of silicon and aluminium, and with the type of glue used to join a device wafer to a support wafer when required, a UV laser is used is used for dopant activation. This solution permits to heat and melt only a shallow depth of silicon for annealing. The p+ layer doping is typically above 10^{18} atoms/cm^3 [8] and its thickness is about 40$\pm$10 nm and

will be referred as the basic passivation throughout this paper. An enhanced passivation consisting of an extra etching process is also available and offers an even thinner p+ layer.

Investigations on devices with similar passivation processes were carried out across a similar broad wavelength range in [9]. However, the products tested in the current trials were adversely affected by an issue with a plasma resist strip process which has been recognised and corrected in the manufacturing line. Therefore the results of the measurements carried out in this paper combined with the data in the soft X-ray spectral range [10] are representative of the devices from these sample wafers but are expected to be lower than typical production. The methods to determine QE reported here will allow determination of the true manufacturing baseline and support future process improvements.

Beyond passivation techniques, Quantum Efficiency enhancement would require additional post-processing such as specific anti-reflective coatings. Such processes are also established at most sensors manufacturers but will not be discussed in this paper.

III. Ultraviolet Quantum Efficiency Measurements of the Passivation Processes

A. The Metrology Light Source M4 Beamline

Quantum Efficiency measurements require maintained standard calibration sources for comparative flux measurements. The selected facility providing reference measurements of monochromatized synchrotron radiation in the UV spectral range is the M4 beamline at the Metrology Light Source (MLS) of the *Physikalisch-Technische-Bundesanstalt* (PTB), located in Berlin (Germany) [11].

The available spectral range spans from 40 nm to 400 nm (31 eV – 3 eV). The photon flux is usually between 10^{10} s^{-1} to 10^{12} s^{-1} but can be reduced to 10^{8} s^{-1} – 10^{9} s^{-1} depending on the wavelength and on the beamline configuration. The flux can be distributed within an area of up to 3 x 2 mm^2 when in focus. The effective beam size depends on the wavelength, on the beamline configuration, and on the focus. In this work, out of focus operation was preferred to minimize the local flux and to prevent non-linearities from pixel saturation.

B. Backside Passivated CCD97

The two levels of passivation performed by Teledyne-e2v [12] at the wafer-level after back-thinning have been tested on back-illuminated CCD97s taken from their standard production line with the exception that no aluminium shielding (optical block) has been applied. The devices substrate is 14 µm thick with an average depletion depth of 2.4 µm. The devices used for this study have been previously used for Quantum Efficiency characterisation in the soft X-ray spectral range [10]. The ultraviolet data presented hereafter allow to fill the gap between the soft X-ray spectrum and the visible spectrum (measurements routinely performed by Teledyne-e2v).

The serial number of the first selected device, with the basic passivation process is 15051-12-44. The serial number of the enhanced passivation device is 15051-07-07. Both devices are uncoated which allows Quantum Efficiency characterisation of the passivation processes only.

C. Camera System and Operation

The selected devices have been operated using the CaVa-Cam system from XCAM Ltd. [13]. This system composed of a DN100CF flange camera head compatible with the ultra-high vacuum requirements of the beamline. The sensors have therefore been operated under vacuum (around 10^{-8} hPa with liquid nitrogen cryo-pumping) at 228 K using thermoelectric cooling (Peltier).

Despite being electron multiplying CCDs (EM-CCD), the CCD97 devices have been operated as standard CCDs. The sensors were continuously readout in time delay integration (TDI) outside the integration periods. For the in-lab ^{55}Fe characterisation an integration time of 5 seconds was set and, for the observation of the spot at the beamline, the integration time was set to 500 ms. Due to the row readout time of 700 µs and the TDI readout mode, the integrated spot has a smeared aspect (see figure 3). Therefore, the data of each row where the spot has not been integrated (e.g. the parallel overscan region) corresponds to the spot signal integrated for the row readout time (700 µs).

The laboratory calibration of the sensors was conducted using a ^{55}Fe soft X-ray source providing two monochromatic spectral lines (Mn-Kα: 5.898 keV and Mn-Kβ: 6.490 keV). 1000 successive frames were acquired allowing the reconstruction of the spectrum. The determined position of Mn-Kα (from a Gaussian fit of the data) in digital numbers (DN) corresponds to a charge of 1616 electrons (assuming an ionizing energy in Silicon of 3.65 eV). Using these two values, it is possible to calculate the calibration factor expressed in e^-/DN.

The Quantum Efficiency measurements across the available spectral range were performed in overlapping subranges due to the different configurations of the beamline. Wavelength steps of 5 nm were chosen for wavelengths between 40 nm and 220 nm. Above and up to 400 nm the sweeps were performed in 10 nm steps.

For each wavelength step, 10 successive frames with 5000 rows have been acquired as well as a reference measurement of the radiative power and photon flux obtained with an absolutely calibrated reference standard photodiode.

D. Obtaining Quantum Efficiency from Images

The Quantum Efficiency for each wavelength acquired is calculated after average electrical offset subtraction using the data in the serial prescan region.

Because of the TDI readout mode, the spot is scanned in the parallel direction in successive steps of 700 µs (row readout time) which results in the smeared aspect in figure 3. During each scanning step, the integrated signal corresponding to the portion of the beam will be added to the previous one. Therefore, the cumulated signal (in digital numbers (DN)) spread across the columns in each row corresponds to the integration of the spot for the row readout time. The total integrated signal during the row readout time is obtained by summing the signal in each pixel of the row. The chosen

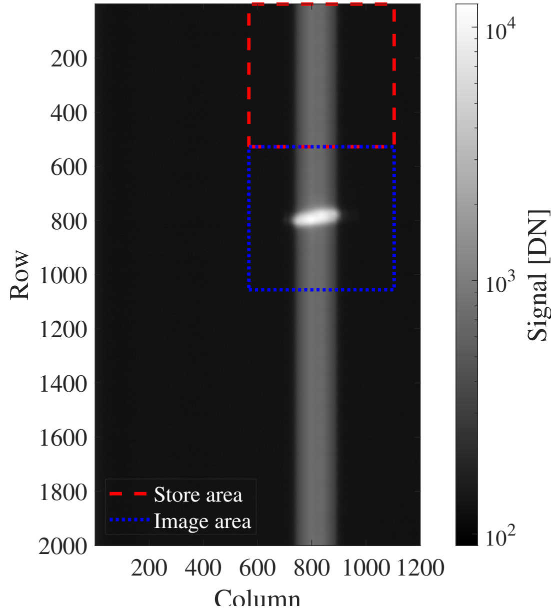

Fig. 3: Image obtained with an enhanced CCD97 (SN: 07-07) readout in TDI mode, resulting in a smeared aspect, following a 500 ms integration of 260 nm photons to observe the shape of the spot at the center of the image area. The total number of rows shown is reduced from 5000 to 2000 for display.

region of interest for the analysis, to avoid the spot acquired by stopping the continuous readout for the integration time, is the parallel overscan region (row $>$ 1056).

The mean signal is averaged over the acquired 10 frames and is converted to electrons per unit time using the row time and the calibration factor from the ^{55}Fe laboratory characterisation.

Because of the variation of the ionisation energy required to produce an electron-hole pair in crystalline silicon in the UV range of the spectrum, the data (in e$^-$/s) cannot be directly converted to a photon flux but requires Quantum Yield (QY) correction. The conversion function has been obtained by fitting published ionisation energy data in the ultraviolet spectrum [14] converted to Quantum Yield.

The Quantum Efficiency is then calculated by comparing the calculated flux (in photons/s) to the measured reference flux. The systematic errors of the reference measurement (2 % — 6 %), of the QY correction method (2 %), as well as the systematic and random errors of the CCD (0.5 % -– 4 %) have been considered for the Quantum Efficiency characterisation.

IV. Results and Discussions

A. Quantum Efficiency

The measured Quantum Efficiency, completing the results from [10], for the back-surface passivation treatments are shown on the right side of figure 4. For wavelengths between 75 nm and 320 nm, where the thickness of the backside potential well and of the native oxide layer, and the reflectivity of the back-surface are the most critical, the characterized Quantum Efficiency remains below 10 % with a minimum of 3.86 % $\pm$ 0.23 % at 100 nm for the basic passivation. Slightly higher efficiency, below 15 %, is observed within the same wide spectral range with the enhanced passivation device. The observed Quantum Efficiency of 7.91 % $\pm$ 0.41 % is observed at 105 nm.

For wavelengths between 70 nm and 370 nm, more than 50 % improvement of the Quantum Efficiency is achieved by the enhanced passivation over the basic process. The efficiency is even doubled in the range 80 nm – 115 nm.

B. Internal Quantum Efficiency

The internal Quantum Efficiency is defined as the number of electrons detected per photon absorbed in the sensitive volume including the native oxide layer and the backside potential well. It is obtained from the measured Quantum Efficiency and the reflectivity at normal incidence R (shown as the red curve in figure 1) [14] using the following relation (with R the total reflectivity and $A_{NativeOxide}$ the absorptance of the native oxide calculated using the refractive indices and extinction coefficients from [3], [4]):

$$QE_{int} = \frac{QE}{1 - R - A_{NativeOxide}} \quad (1)$$

With a sufficiently thin p+ layer, almost 100 % internal Quantum Efficiency is possible (e.g. with delta-doping [7]).

The two passivation levels presented in this work do not achieve 100 % internal Quantum Efficiency (figure 5) but remain limited to maximum values around 45 % with the enhanced passivation device for wavelengths between 145 nm and 165 nm. The values for the basic passivation process do not exceed 25 % within the same spectral range.

C. Effects Due to Long Exposures

To observe the effects of intense high flux UV exposures, the devices have been exposed to high flux of 200 nm radiation, using the M4 beamline, for several hours. Quantum Efficiency measurements have been repeated after few hours of exposure. Intermediate measurements were limited to the wavelengths available with the beam configuration. A full sweep has been performed after the total cumulated exposure. The Quantum Efficiency variations with different exposure times for the enhanced device are shown in figure 6.

After two hours illumination, an increase of the Quantum Efficiency (approximatively 1.6 $\times$ at 285 nm) has been observed without further change for the next 15 hours. Similar effect to a lesser degree has been observed with the basic passivation device.

As the illumination was performed using the spot, portions of the image area remained unilluminated. Limited spectral range Quantum Efficiency measurements were performed in a dark area as a control. A small change has been observed.

The long exposures may have affected the reflectivity properties by adding or removing contamination at the surface or may have improved the internal Quantum Efficiency by negative charging of the oxide layer (QE-pinning [1]). The rapid change followed by stable performance with continuing exposure tends to rule out accumulating contamination material. Negative charging is considered the most likely cause, but the reflectivity change cannot be ruled out without additional measurements.

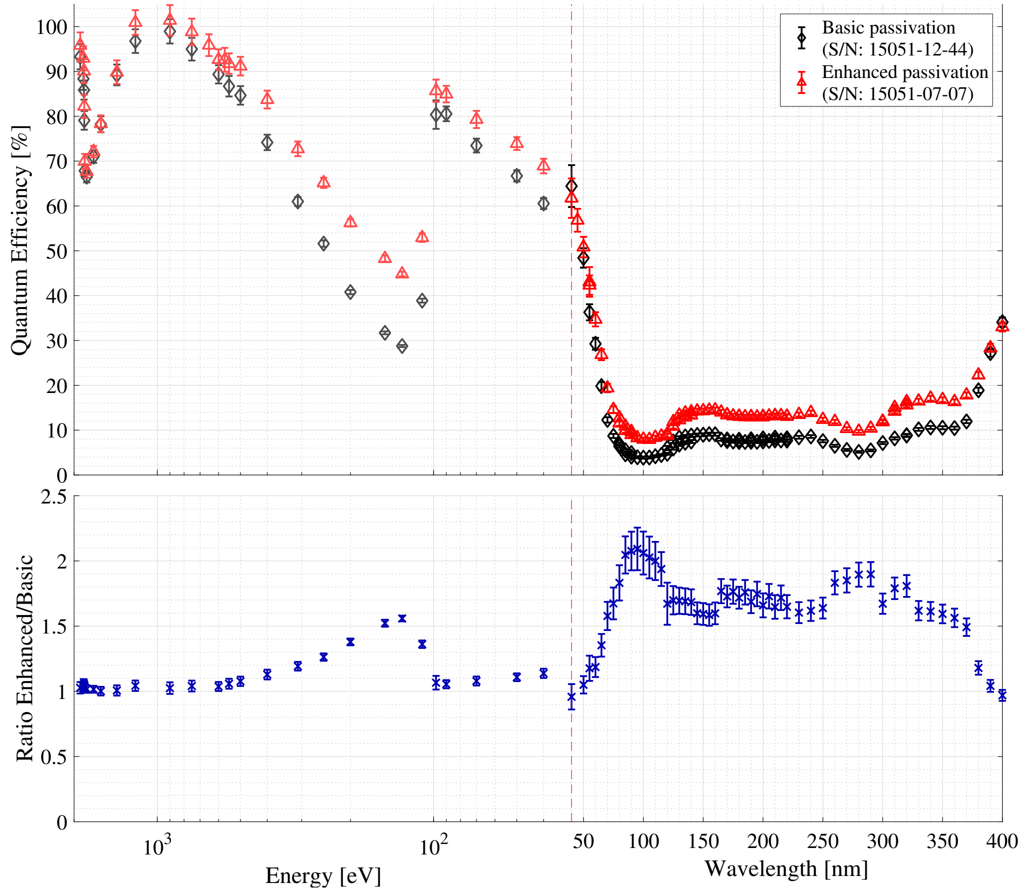

Fig. 4: Top: Quantum Efficiency measured for the two backside passivation processes applied on back-thinned CCD97 (basic: black diamonds; enhanced: red triangles). Bottom: ratio between the enhanced and the basic versions of the passivation process. The red dashed line delimits the data from [10] on the left side with the logarithmic x-axis, and from the present work on the right side with the linear x-axis. The discrepancy at the junction is due to higher errors at the shortest wavelengths tested in the ultraviolet spectral range.

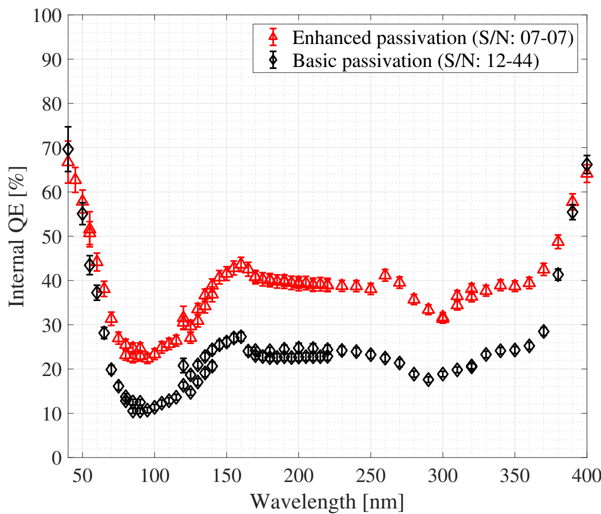

Fig. 5: Internal Quantum Efficiency obtained after conversion of the data in figure 4 using equation 1.

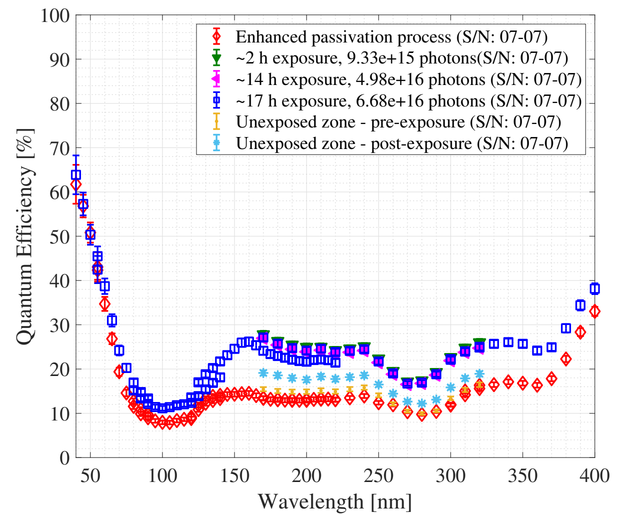

Fig. 6: Comparative Quantum Efficiency measurements performed with an enhanced passivation device before and after intense UV (200 nm) illumination.

V. Conclusions and Future Work

In this work, a method to measure the quantum efficiency in the ultraviolet range has been established. Along with previous work reported in the soft X-ray range reported in [10] and more common measurements available in the visible range characterisation of Quantum Efficiency response across a very wide wavelength has been established and will be useful in characterising manufacture baseline performance and potential process improvements and to test physical models of Quantum Efficiency.

The measurements have been applied to two passivation process types available from Teledyne-e2v. The basic passivation process consists of a low-energy boron implantation at the back-surface followed by ultraviolet laser annealing providing a 40 nm$\pm$10 nm thick p+ layer (doped above 10^{18} atoms/cm^3). The enhanced process consisting of an additional etching of the implanted back-surface provides an even thinner p+ layer.

The measurements were conducted with wavelengths ranging from 40 nm to 400 nm. An efficiency up to 15 % at the most challenging wavelengths close to 285 nm where the absorption length is short, and the reflectivity is high has been measured for the enhanced process. Overall, in the most critical spectral range (70 nm–370 nm), the enhanced passivation process offers more than 50 % higher Quantum Efficiency compared to the basic process.

With imperfect internal Quantum Efficiency and a p+ passivation layer, an effect of temperature on internal Quantum Efficiency is expected, especially at lower temperatures. Therefore, additional characterisation work of passivated devices could include comparative Quantum Efficiency measurements at different operating temperatures.

Also, the measurements conducted in this work were at normal incidence. Further work could include Quantum Efficiency characterisation of the processes at various incident angles to provide reference values for applications with isotropic illumination.

The devices were exposed to long high flux Ultraviolet exposures to observe any change. An increase of the Quantum Efficiency has been observed with both processes. The determination of the cause would require additional measurements and studies such as reflectivity measurements as well as carrier lifetime measurements.

Quantum Efficiency characterisation of anti-reflective coatings within the same spectral range as well as the effect of lifetime levels of UV exposure on Quantum Efficiency will be conducted. The results will be presented subsequently. The results will provide useful calibration of the processes for current and future space, scientific and industrial applications.

References

[1] J. R. Janesick, *Scientific Charge-Coupled Devices*. SPIE, Jan. 2001.

[2] M. Bass, C. DeCusatis, J. M. Enoch, V. Lakshminarayanan, G. Li, C. MacDonald, V. N. Mahajan, and E. V. Stryland, *Handbook of Optics, Third Edition Volume I: Geometrical and Physical Optics, Polarized Light, Components and Instruments(set)*. McGraw-Hill Education, 2009.

[3] E. D. Palik, *Handbook of Optical Constants of Solids*. Elsevier, 1985.

[4] ——, *Handbook of Optical Constants of Solids, Vol. 2*. Academic Press, 1991.

[5] Teledyne-e2v, Private communication.

[6] M. A. Green and M. J. Keevers, “Optical properties of intrinsic silicon at 300 K,” *Progress in Photovoltaics: Research and Applications*, vol. 3, no. 3, pp. 189–192, 1995. [Online]. Available: https://onlinelibrary.wiley.com/doi/abs/10.1002/pip.4670030303

[7] M. E. Hoenk, T. J. Jones, M. R. Dickie, F. Greer, T. J. Cunningham, E. R. Blazejewski, and S. Nikzad, “Delta-doped back-illuminated CMOS imaging arrays: progress and prospects,” in *Infrared Systems and Photoelectronic Technology IV*, E. L. Dereniak, J. P. Hartke, P. D. LeVan, R. E. Longshore, and A. K. Sood, Eds. SPIE, Aug. 2009.

[8] P. Jerram, D. Burt, N. Guyatt, V. Hibon, J. Vaillant, and Y. Henrion, “Back-thinned CMOS sensor optimization,” in *Optical Components and Materials VII*, S. Jiang, M. J. F. Digonnet, J. W. Glesener, and J. C. Dries, Eds., vol. 7598, International Society for Optics and Photonics. SPIE, 2010, pp. 298 – 309. [Online]. Available: https://doi.org/10.1117/12.852389

[9] R. A. Stern, L. Shing, P. R. Catura, M. D. Morrison, D. W. Duncan, J. R. Lemen, T. Eaton, P. J. Pool, R. Steward, D. M. Walton, and A. Smith, “Characterization of the flight CCD detectors for the GOES N and O solar x-ray imagers,” in *Telescopes and Instrumentation for Solar Astrophysics*, S. Fineschi and M. A. Gummin, Eds., vol. 5171, International Society for Optics and Photonics. SPIE, 2004, pp. 77 – 88. [Online]. Available: https://doi.org/10.1117/12.506346

[10] I. Moody, M. Watkins, R. Bell, M. Soman, J. Keelan, and A. Holland, “CCD QE in the Soft X-ray Range,” e2v Technologies, Tech. Rep., 2017.

[11] A. Gottwald, U. Kroth, M. Richter, H. Schöppe, and G. Ulm, “Ultraviolet and vacuum-ultraviolet detector-based radiometry at the Metrology Light Source,” *Measurement Science and Technology*, vol. 21, no. 12, p. 125101, oct 2010.

[12] Teledyne-e2v. [Online]. Available: https://imaging.teledyne-e2v.com/

[13] XCAM. [Online]. Available: http://www.xcam.co.uk

[14] P. Kuschnerus, H. Rabus, M. Richter, F. Scholze, L. Werner, and G. Ulm, “Characterization of photodiodes as transfer detector standards in the 120 nm to 600 nm spectral range,” *Metrologia*, vol. 35, no. 4, pp. 355–362, aug 1998.